Acta Crystallographica Section B
Structural Science
ISSN 0108-7681

Single-crystal X-ray diffraction and electron-microscopy study of multiple-twinned $Sr_3(Ru_{0.336},Pt_{0.664})CuO_6$

Karen Friese,* Lorenz Kienle, Viola Duppel, Hongmei Luo and Chengtian Lin

Max-Planck-Institut für Festkörperforschung, Heisenbergstrasse 1, D-70569 Stuttgart, Germany

Correspondence e-mail: k.friese@fkf.mpg.de

Received 2 October 2002
Accepted 23 December 2002

$Sr_3(Ru_{0.336},Pt_{0.664})CuO_6$ crystallizes as a monoclinic structure [space group $R12/c$; lattice parameters $a = 9.595\,(15)$, $b = 9.595\,(15)$, $c = 11.193\,(2)$ Å and $\gamma = 120^\circ$]. The crystal structure is pseudotrigonal and the crystal investigated here by single-crystal X-ray diffraction was a multiple twin composed of six individuals. The twin laws are a combination of rhombohedral obverse/reverse twinning plus the threefold axis from the trigonal system. The crystal structure is related to the hexagonal perovskites. Each Pt/Ru atom is coordinated pseudo-octahedrally by O atoms, while the overall coordination polyhedra for Cu atoms can be regarded as a strongly distorted trigonal prism, where the Cu atom is clearly shifted from the center. Each $[(Ru_{0.336},Pt_{0.664})O_6]$ octahedron is connected to two Cu—O polyhedra *via* a common edge, and thus chains are formed parallel to the crystallographic c axis. Sr^{2+} ions are incorporated between the chains and are coordinated by eight O atoms. All bond distances and angles are in good agreement with literature values. Electron-microscopy studies confirm the results from X-ray diffraction and all observed domain structures can be interpreted exactly with the established twin model. No indication of Pt/Ru ordering was found in either the X-ray or the electron-microscopy investigation.

1. Introduction

In recent years, interest in hexagonal perovskites and their related structures has been growing rapidly. Numerous compounds have been investigated and described either as intergrowth compounds in higher-dimensional space or as compounds formed by the stacking of mixed layers.

Very few copper-containing compounds are, to our knowledge, found in the perovskite family. Examples that have been characterized structurally are $La_2(Cu_{0.96}Ti_{1.04})O_6$ (*Pnma*; Palacin *et al.*, 1994), $NdCu_3(Ti_3Fe)O_{12}$ ($Im\bar{3}$; Meyer *et al.*, 1978) and $Ca_{1.75}Sr_{1.5}Cu_{0.75}PtO_6$ ($R\bar{3}c$; Bykov *et al.*, 1990).

Because the number of well characterized copper-containing perovskites is small, and given the importance of the Sr/Ru/(Pt)/Cu system for the investigation of superconducting materials, we chose to investigate a new perovskite-related material, $Sr_3(Ru_{0.336},Pt_{0.664})CuO_6$, in detail using a combined methodical approach of single-crystal X-ray diffraction and transmission electron microscopy.

Table 1
Basic parameters for HRTEM.

Voltage (kV)	300
Cathode	LaB_6
Spherical aberration constant (C_S; mm)	1.15
Maximum point resolution (Å)	1.9
Spread of defocus (Å)	70
Illumination semiangle (mrad)	1.2
Tilting maximum (double tilt holder; °)	±25

2. Experimental

2.1. Synthesis

Crystals were obtained as a by-product during a systematic exploration of the system Ru/Sr/Gd/Cu/O, for which the self-flux method was employed. Mixtures of RuO_2, $SrCO_3$, CuO and Gd_2O_3 (Ru:Sr:Gd:Cu = 1.8:2:1.4:3.7) were treated as described by Lin *et al.* (2001). The Pt content that is incorporated in the crystals originates from the Pt crucible in which the single crystals were obtained.

2.2. Electron microscopy

A selected crystal was crushed and suspended in *n*-butanol. A perforated carbon–copper net was covered with the suspension, and wedge-shaped fragments of the crystal were left in random orientations after drying. High-resolution transmission electron microscopy (HRTEM) and selected-area electron diffraction (SAED) were performed with a Philips CM30/ST microscope (for basic parameters see Table 1). HRTEM images and SAED patterns were registered with a Gatan slow-scan CCD camera (*Digital Micrograph* 2.5 software).

Computer simulations of electron diffraction patterns (kinematical approximation) and HRTEM images (multislice formalism) were calculated with the *EMS* program package (Stadelmann, 1987). The basis of all simulations was the structure model presented below. The atomic parameters of the non-standard setting $R12/c$ were transformed to $P1$. After Fourier transformation, a suitable band-pass mask was used to reduce noise in the HRTEM micrographs. The image-processing procedures that were implemented in order to highlight the domain structure of the crystal fragments are discussed in the text. EDX (energy-dispersive X-ray diffraction) data (SiLi detector, Noran) were analyzed with the Vantage DSI system (Noran).

2.3. X-ray diffraction

Single-crystal diffraction intensities were collected with a Stoe STADI4 diffractometer in combination with an Oxford CCD camera. Experimental details are given in Table 2.[1]

[1] Supplementary data for this paper are available from the IUCr electronic archives (Reference: NA0140). Services for accessing these data are described at the back of the journal.

Table 2
Experimental details.

Crystal data	
Chemical formula	$Cu_{0.5}O_3Pt_{0.332}Ru_{0.168}Sr_{1.5}$
M_r	293.08
Cell setting, space group	Monoclinc, $R12/c$
Symmetry operations	(0, 0, 0)+; $(\frac{2}{3},\frac{1}{3},\frac{1}{3})$+; $(\frac{1}{3},\frac{2}{3},\frac{2}{3})$+; $\pm x, y, z$; $\pm y, x, \frac{1}{2}-z$
a, b, c (Å)	9.595 (15), 9.595 (15), 11.193 (2)
α, β, γ (°)	90, 90, 120
V (Å^3)	892.4 (3)
Z	18
D_x (Mg m^{-3})	6.539
Radiation type	Mo $K\alpha$
No. of reflections for cell parameters	27 773
θ range (°)	4–36.8
μ (mm^{-1})	46.6
Temperature (K)	293 (2)
Crystal form, color	Hexagonal prismatic, colorless
Crystal size (mm)	0.08 × 0.04 × 0.02
Approximated by	17 faces
Data collection	
Diffractometer	Stoe STADI4; Oxford Instrument KM4 CCD Sapphire
Exposure time per frame (s)	90
Detector distance (mm)	48.65
Absorption correction	Gaussian
T_{min}	0.034
T_{max}	0.104
No. of measured, independent and observed parameters	27 773, 4822, 3201
Criterion for observed reflections	$I > 3\sigma(I)$
θ_{max} (°)	36.8
Range of h, k, l	$-15 \Rightarrow h \Rightarrow 16$ $-16 \Rightarrow k \Rightarrow 15$ $-19 \Rightarrow l \Rightarrow 18$
Refinement	
Refinement on	F^2
$R[F^2 > 2\sigma(F^2)]$, $wR(F^2)$, S	0.057, 0.050, 3.23
R(all), wR(all), S(all)	0.084, 0.050, 2.65
No. of reflections	4822 reflections
No. of parameters	55
Twin matrix I	1 0 0 / 0 1 0 / 0 0 1
Twin matrix II	−1 0 0 / 0 −1 0 / 0 0 1
Twin matrix III	0 −1 0 / 1 −1 0 / 0 0 1
Twin matrix IV	−1 1 0 / −1 0 0 / 0 0 1
Twin matrix V	0 1 0 / −1 1 0 / 0 0 1
Twin matrix VI	1 −1 0 / 1 0 0 / 0 0 1
Twin volume fraction I	0.093 (6)
Twin volume fraction II	0.337 (3)
Twin volume fraction III	0.090 (2)
Twin volume fraction IV	0.150 (2)
Twin volume fraction V	0.217 (3)
Twin volume fraction VI	0.113 (3)
Weighting scheme	Calculated $w = 1/[\sigma^2(F_o^2)]$
$(\Delta/\sigma)_{max}$	< 0.0001
$\Delta\rho_{max}$, $\Delta\rho_{min}$ (e Å^{-3})	18.59, −5.24
Extinction method	Isotropic
Extinction coefficient	0.0099 (5)

Computer programs: *XCALIBUR* (Oxford Diffraction, 2000), *X-RED* (Stoe & Cie, 1998), *SIR*97 (Altomare *et al.*, 1997), *JANA*2000 (Petříček & Dušek, 2000).

3. Structure determination

In the diffraction experiments, we only observed intensities for reflections with $-h + k + l = 3n$ and $h - k + l = 3n$. These reflections correspond to the two extinction rules for an R

Table 3
Selected bond distances and angles (Å, °) around Sr^{2+} for $Sr_3(Ru_{0336},Pt_{0664})CuO_6$ at room temperature.

Sr1	O3	2.457 (14)	Sr1	O2	2.466 (10)
	O1	2.491 (14)		O1	2.626 (12)
	O3	2.652 (13)		O2	2.656 (15)
	O1	2.701 (11)		O3	2.761 (13)
Sr2	O2	2 × 2.460 (10)	Sr2	O2	2 × 2.600 (15)
	O3	2 × 2.734 (13)		O1	2 × 2.791 (13)
O3—Sr1—O2		130.4 (5)	O3—Sr1—O1		73.1 (4)
O3—Sr1—O1		96.3 (4)	O3—Sr1—O3		73.0 (5)
O3—Sr1—O2		138.8 (4)	O3—Sr1—O1		119.2 (4)
O3—Sr1—O3		76.2 (4)	O2—Sr1—O1		74.8 (4)
O2—Sr1—O1		114.0 (4)	O2—Sr1—O3		152.3 (4)
O2—Sr1—O2		90.6 (4)	O2—Sr1—O1		67.4 (4)
O2—Sr1—O3		67.5 (4)	O1—Sr1—O1		79.9 (4)
O1—Sr1—O3		131.9 (3)	O1—Sr1—O2		131.2 (4)
O1—Sr1—O1		137.9 (4)	O1—Sr1—O3		90.9 (4)
O1—Sr1—O3		71.1 (4)	O1—Sr1—O2		63.8 (4)
O1—Sr1—O1		132.2 (5)	O1—Sr1—O3		169.6 (5)
O3—Sr1—O2		66.6 (4)	O3—Sr1—O1		88.8 (4)
O3—Sr1—O3		112.7 (4)	O2—Sr1—O1		68.4 (4)
O2—Sr1—O3		126.5 (4)	O1—Sr1—O3		58.2 (5)
O2—Sr2—O2		90.0 (3)	O2—Sr2—O2		2 × 79.0 (4)
O2—Sr2—O3		2 × 116.7 (4)	O2—Sr2—O3		2 × 136.6 (4)
O2—Sr2—O1		2 × 136.4 (4)	O2—Sr2—O1		2 × 69.7 (4)
O2—Sr2—O2		92.1 (4)	O2—Sr2—O2		167.4 (3)
O2—Sr2—O3		2 × 129.3 (4)	O2—Sr2—O3		2 × 63.2 (4)
O2—Sr2—O1		2 × 64.3 (4)	O2—Sr2—O1		2 × 119.5 (4)
O3—Sr2—O3		67.6 (4)	O3—Sr2—O1		2 × 67.5 (4)
O3—Sr2—O1		2 × 86.6 (4)	O1—Sr2—O1		149.1 (3)

Table 4
Selected bond distances and angles (Å, °) around Ru/Pt and Cu for $Sr_3(Ru_{0336},Pt_{0664})CuO_6$ at room temperature.

Ru/Pt	O2	2 × 1.992 (9)	Cu	O1	2 × 1.983 (14)
	O1	2 × 2.014 (14)		O3	2 × 2.010 (14)
	O3	2 × 2.044 (13)		O2	2 × 2.785 (9)
O2—Pt—O2		180.0	O1—Cu—O1		171.9 (4)
O2—Pt—O1		2 × 88.4 (4)	O1—Cu—O3		2 × 83.4 (6)
O2—Pt—O1		2 × 91.6 (4)	O1—Cu—O3		2 × 95.1 (6)
O2—Pt—O3		2 × 87.6 (4)	O1—Cu—O2		69.4 (6)
O2—Pt—O3		92.4 (4)	O1—Cu—O2		117.5 (4)
O1—Pt—O1		180.0	O3—Cu—O3		158.1 (4)
O1—Pt—O3		81.7 (6)	O3—Cu—O2		69.2 (4)
O1—Pt—O3		98.3 (6)	O3—Cu—O2		130.7 (4)
O3—Pt—O3		180.0	O2—Cu—O2		77.3 (3)

Table 5
Bond-valence sums calculated according to Brese & O'Keeffe (1991).

Sr1	O1	Sr2	O2	$Ru_{0.334}Pt_{0.666}$	O3	Cu
2.26	2.10	2.04	2.05	3.98	2.03	1.80

lattice: $-h+k+l=3n$ is the extinction rule for a rhombohedral lattice in the obverse setting, while $h-k+l=3n$ is the rule for the reverse setting. Thus it was obvious from the beginning that the investigated crystal is a twin and comprises two rhombohedral lattices that can be transformed into each other *via* the application of a twofold rotation axis around [001].

Furthermore, we observed extinction rules that are in agreement with a *c*-glide plane ($hh\bar{0}l$: $l=2n+1$) for both twin individuals, which leads to the extinction symbol $R-c$. We were able to solve the structure with the reflections corresponding to one rhombohedral lattice in space group $R\bar{3}c$ *via* direct methods (*SIR*97; Altomare *et al.*, 1997) without major problems, although the intensities of reflections with $l=3n$ are naturally falsified because of the contribution of the second twin individual.

This solution yielded the positions of the heavy atoms. Using the program *JANA*2000 (Petříček & Dušek, 2000), and taking into account the obverse/reverse twinning in the structure refinement, we were then able to locate the O atoms *via* subsequent difference Fourier synthesis.

It transpired during the refinement that the Cu atom, which we assumed to be located on the threefold axis [Wyckoff position 6(*a*): 0, 0, 1/4 of $R\bar{3}c$ in the hexagonal setting], was slightly shifted from this position to a more general (x, x, z) position, thus breaking the overall threefold symmetry. In principle, there are two approaches to describing this situation: (i) a split-atom model that maintains the higher symmetry $R\bar{3}c$ or (ii) a twin model that assumes the crystal is composed of three individuals of lower symmetry, which are related *via* the threefold axis. In the case of $Sr_3(Ru_{0.336},Pt_{0.664})CuO_6$, however, only the second approach is possible, as became evident when we looked at the electron-density map around the Cu-atom site, took into account the unmerged data, assumed the symmetry *R*1 and calculated phases from the model with the Cu atom at 0, 0, *z*. Three different maxima corresponding to Cu-atom positions at approximately (i) −0.05, −0.05, 0.249, (ii) 0.05, 0, 0.249 and (iii) 0, 0.05, 0.249 are clearly discernible in this map. As the three maxima have significantly different heights, it is not possible to keep the threefold axis in the model, since retaining this axis would always lead to three maxima of the same height. Therefore, we were forced to lower the symmetry further. Choosing the symmetry operations $\pm x, y, z$ and $\pm y, x, \bar{z}+\frac{1}{2}$ of the space group $R\bar{3}c$ we arrived at the space group *R*12/*c* (a non-standard setting of the space group *C*2/*c*; see *Appendix A*). Four additional twin individuals had to be introduced (see Table 2). The unconventional space group was chosen to maintain the close relation to the higher trigonal pseudosymmetry and to the hexagonal perovskites in general.[2]

Altogether, six domains and their corresponding twin matrices have to be taken into account. The six matrices and their corresponding volume fractions as obtained from the refinement are given in Table 2. The obverse setting corresponds to about one-third of the volume and the reverse setting allows for the other two thirds.

No indication was found of any Ru/Pt ordering, and we thus assumed that the two species were distributed statistically on the same site.

Details concerning the refinement are given in Table 2, selected distances and angles are given in Tables 3 and 4. Lattice parameters and transformation matrices are given in

[2] Note that although the lattice parameters refined from single-crystal data are trigonal within the experimental errors, a LeBail fit of powder data shows a slight deviation from the trigonal metrics, which leads to a monoclinic cell [$a=9.628$ (2), $b=9.612$ (2), $c=11.241$ (1) Å and $\beta=119.87$ (3)°].

Appendix A. Atomic coordinates in the standard setting *C*2/*c* are available as part of the supplementary material.

4. Electron microscopy

Initially defect-free fragments of the examined crystal were checked by HRTEM and electron diffraction for deviations from the structural model derived from the X-ray diffraction (XRD) analysis. The diffraction patterns obtained by tilting experiments can be completely indexed on the basis of the results of the XRD analysis. All tilt angles between different crystal orientations were consistent with the metrics of this model.

The existence of *R*-centering was confirmed by electron diffraction using a parallel and a convergent electron beam (the latter for the inspection of higher-order Laue zones, *e.g.* the first-order Laue zone for zone axis [001]). Images with variable defocus of several zone axes indicate no significant structural deviation from the model obtained by XRD methods. A typical example is depicted in Fig. 1 for zone axis [001]; the simulated images are shown as insets in the experimental images. There are no variations of the contrasts that give any evidence for a local ordering of Ru or Pt (see also X-ray experiments).

Apart from the defect-free fragments, we also examined many fragments that are characterized by lamellar domains.

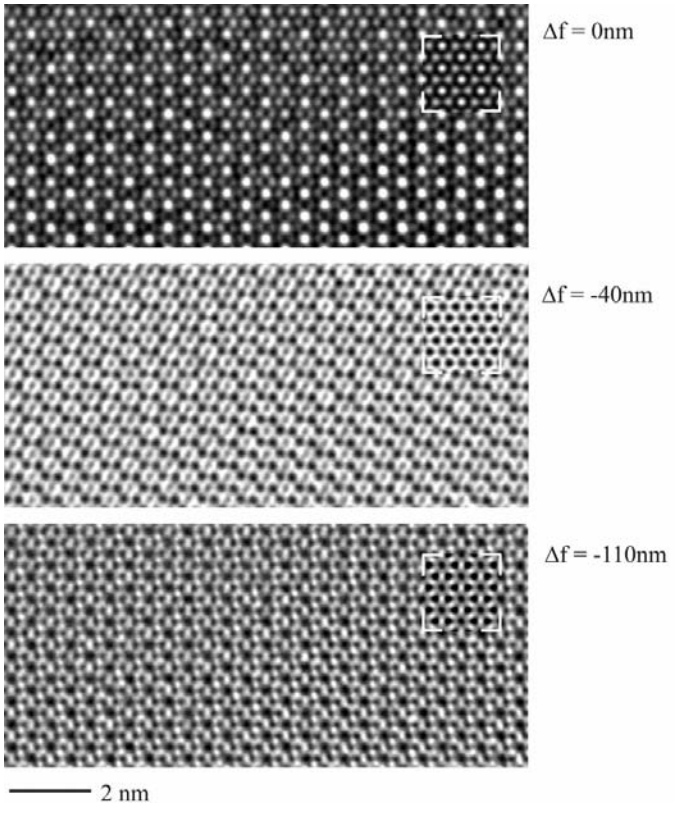

Figure 1
Series of HRTEM micrographs (zone axis [001]), with inserted simulations (thickness = 2.2 nm). The values of the defocus are depicted on the right-hand side

The two main features of these domain crystals are presented in Figs. 2 and 3. As shown in the bright-field image of Fig. 2(*a*), many of the examined fragments are clearly striped. Alternating brighter and darker stripes were also observed in dark-field images with reversed contrast. As indicated by electron diffraction and Fourier transforms of HRTEM micrographs, the boundaries between brighter and darker stripes are exactly aligned in the [001] direction. A remarkable difference becomes evident when fast Fourier transforms (FFTs) of square regions of both types of stripes are calculated. The dark stripe [in the upper half of Fig. 2(*b*)] exhibits reflections with $l = 2n + 1$, while the FFT of the neighboring brighter stripe does not. This observation can be interpreted on the basis of the twinning model that was described above. A fundamental feature of this multiple-twinning model is the coexistence of six possible crystal orientations, which exhibit different diffraction patterns when looked at individually. There are four patterns with significant intensities for reflections with $l = 2n + 1$ (*i.e.* [100], [$\bar{1}$00], [010] and [0$\bar{1}$0]) and two without intensities for these reflections ([110] and [$\bar{1}\bar{1}$0]). The differ-

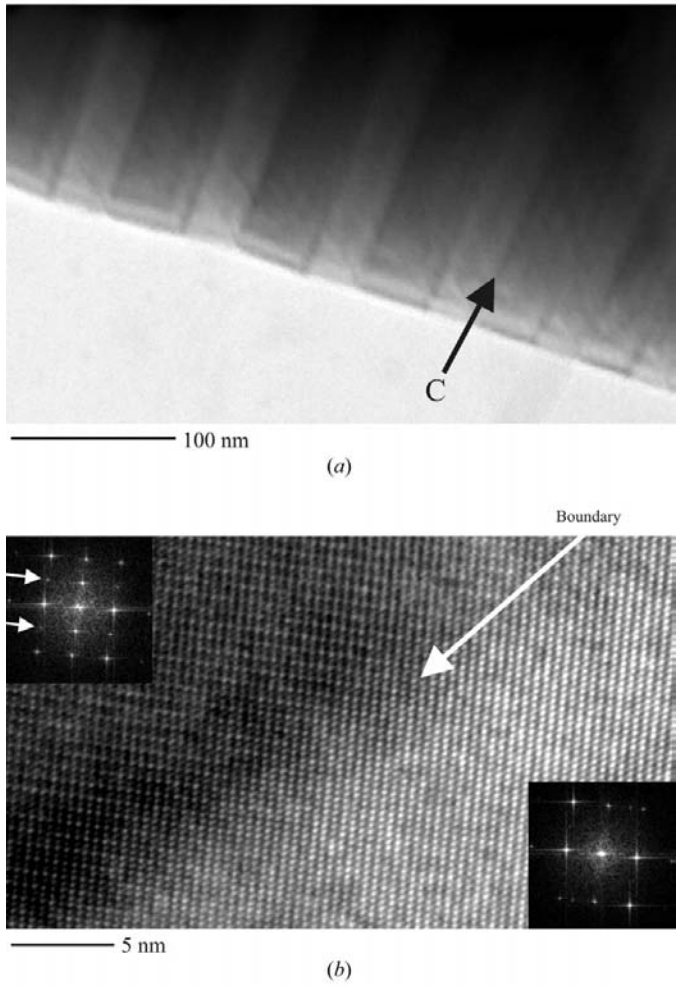

Figure 2
(*a*) Bright-field image, taken on a fragment of the observed crystal (aligned in [100]). Well separated darker and brighter stripes are apparent. (*b*) HRTEM micrograph of the boundary between darker and brighter stripes, with inserted FFTs.

ence in contrast (brighter and darker stripes) can be explained by diffraction contrast only, *i.e.* the bright and dark stripes represent separated twin lamellae with different orientations (*e.g.* [100] including reflections *hkl* with $l = 2n + 1$ and [110] without these reflections).

This hypothesis is supported by diffraction experiments (Fig. 3*a*). In the case of the broad stripes, the patterns of brighter and darker stripes can be recorded sequentially when the SAED aperture is shifted over an aligned crystal. We observed good agreement (*e.g.* for zone axes [100] and [110] for the neighboring twin lamellae) between simulations and the experimental patterns when we examined the thin regions of the stripes. Image-processing methods can be applied to highlight the differently orientated lamellae (see Fig. 3*b*). Starting from the FFT of a square region of the whole image of Fig. 2(*b*), the peaks with $l = 2n + 1$ can be separated using a suitable mask. In the second step, a processed image is calculated by inverse FFT using the reflections with $l = 2n + 1$ only. The resulting image (see Fig. 3*b*) shows artifacts due to the filtering, but this image does verify the presence of separated twin lamellae. Observations of many fragments show that the width of the twin lamellae is 10–200 nm.

An analysis of the atomic structure at the twin interface indicates no structural distortion between differently orientated domains, and diffuse scattering was not observed. The region between a darker and a brighter stripe is displayed in a high-resolution micrograph in Fig. 4. On the upper left-hand side of the image, one lamella is aligned perpendicular to the

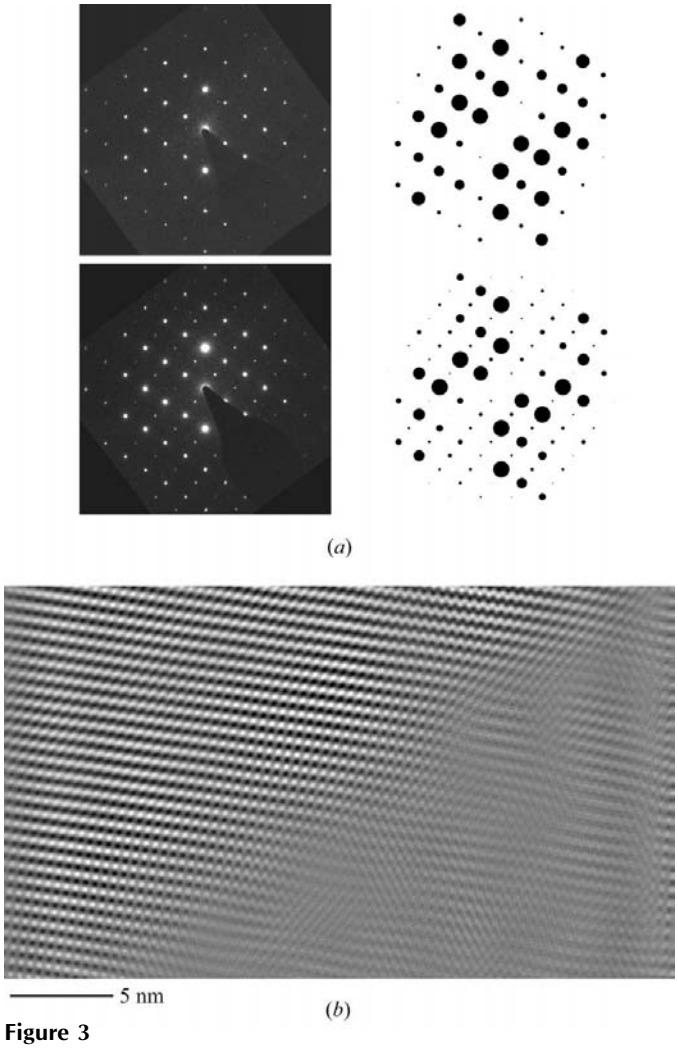

Figure 3
(*a*) Diffraction patterns recorded on neighboring lamellae (left) and simulations of the diffraction patterns (right). (*b*) Image depicted in Fig. 2(*b*) after image processing (see text).

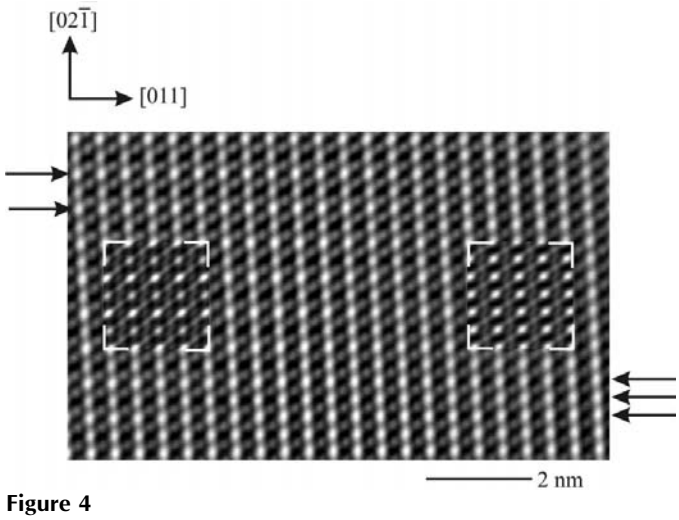

Figure 4
HRTEM micrograph taken at the boundary between a darker and brighter stripe. Simulations of the images are inserted (left: zone axis [100]; right: zone axis [110]; $\Delta f = -30$ nm; thickness = 7.7 nm). The arrows highlight vertical lines of spots with equal intensity.

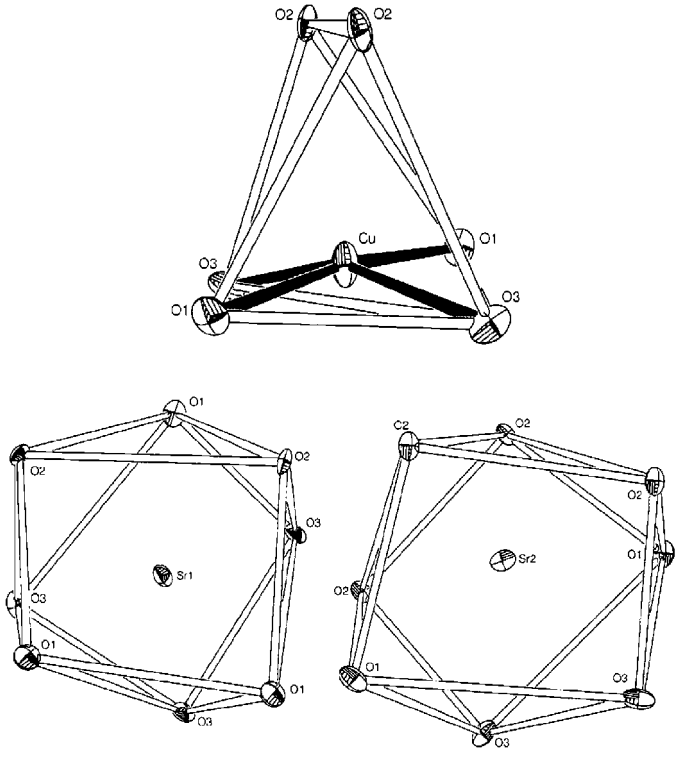

Figure 5
The cation coordination polyhedra realized in $Sr_2(Ru_{0.336},Pt_{0.664})CuO_6$. Figure drawn with *ORTEP*3 *for Windows* (Farrugia, 1997).

zone axis [100]. As indicated by the convincing agreement between the experimental image and the simulated one, there are significant differences in the contrasts along [02$\bar{1}$], and rows of brighter and darker points alternate parallel to [011] (see arrows in Fig. 4). On the right -hand side of the image, the orientation of the neighboring lamella is switched to, for example, [110], and the differences in contrast discussed above vanish. Hence, the distance between rows of bright spots is halved. Again, this result is in good agreement with the simulated image (right-hand side of Fig. 4).

Many crystallites were checked by EDX for variations of the stoichiometry. All point analyses indicate a minor content of Gd (>1 at%) in the crystals and an approximate ratio of Ru:Pt of 1:2.5–3.0. According to our observations (XRD mapping, line scans and analyses of selected points of the brighter and darker stripes), both types of stripes contain equal amounts of the detectable elements (Pt, Ru, Sr). XRD mapping indicates a homogeneous distribution of each of these three elements in the area of a striped crystallite. In particular, no inhomogenities were observed at the boundaries of the stripes, thus confirming that the variations in contrast (bright and dark stripes) are due to diffraction contrast only.

5. Crystal structure and discussion

The structure of the investigated compound is closely related to the structure of the hexagonal perovskites. Numerous compounds belonging to this family have been described in the literature. The most important difference between them is the individual building unit that can be derived from the chain of face-sharing octahedra in the ideal perovskite structure. Octahedra can be replaced by trigonal prisms in hexagonal perovskite structures, and the chains are then composed of different sequences of octahedra and trigonal prisms. Detailed discussions about the hexagonal perovskites and their related structures can be found in the literature (Abakumov *et al.*, 1998; Boulahya *et al.*, 1999; Elcoro *et al.*, 2000, 2001; Floros *et al.*, 2000; Gourdon *et al.*, 1999, 2000; Grasset *et al.*, 1998; Renard *et al.*, 1999).

In the title compound, each Pt/Ru is pseudo-octahedrally coordinated by O atoms, with bond distances of 1.99–2.04 Å, which are in good agreement with the distances given for comparable compounds in the literature [$Ca_{1.75}Sr_{1.5}Cu_{0.75}PtO_6$: 2.028 Å (Bykov *et al.*, 1990); $Sr_4Ru_{3.05}O_{12}$: 1.94 (3)–2.04 (5) (Renard *et al.*, 1999)].

On the other hand, the coordination of Cu atoms by O atoms can be described as (4 + 2): the four nearest neighbors are at distances of 1.983–2.010 Å. These four O atoms form a square planar coordination. The Cu atom, however, is not

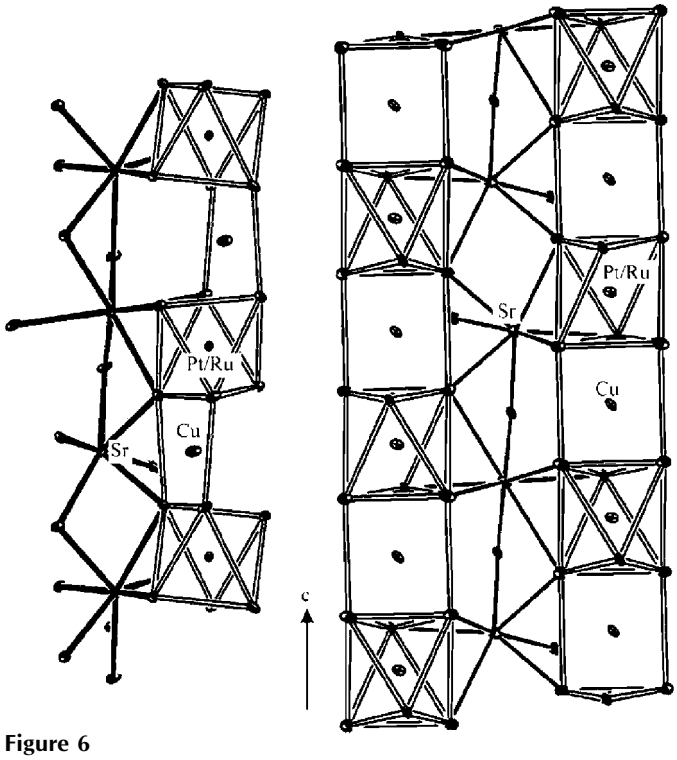

Figure 6
Two partial views of the chain of octahedra and Cu-coordination polyhedra in $Sr_2(Ru_{0.336},Pt_{0.664})CuO_6$. (Left) View along [100]; (right) view along [110]. Sr—O bonds are indicated by thick black lines. Figure drawn with *ORTEP*3 *for Windows* (Farrugia, 1997).

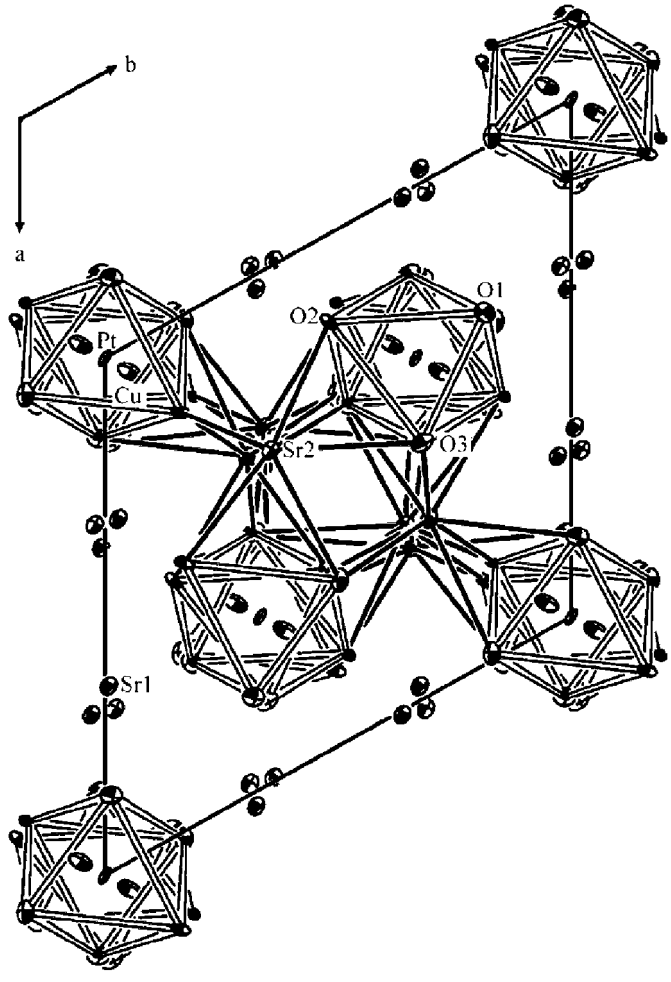

Figure 7
Projection along [001] of the structure of $Sr_2(Ru_{0.336},Pt_{0.664})CuO_6$. $(Ru/Pt)O_6$ octahedra are indicated. Sr—O bonds are indicated by thick black lines. Figure drawn with *ORTEP*3 *for Windows* (Farrugia, 1997).

exactly in the center of the square but is slightly shifted in the direction of the remaining two O atoms (at distances of 2.785 Å, see Fig. 5). The overall coordination polyhedron can be regarded as a strongly distorted trigonal prism, where the Cu atom is clearly shifted from the center.

A similar coordination for copper is observed in $Ca_{1.75}Sr_{1.5}Cu_{0.75}PtO_6$ (Bykov *et al.*, 1990). In $NdCu_3(Ti_3Fe)O_{12}$ (Meyer *et al.*, 1978) on the other hand, the Cu atoms again have four nearest neighbors but have four additional O atoms at larger distances.

Both symmetrically independent Sr atoms are coordinated by eight O atoms (see Fig. 5), with distances of 2.457–2.791 Å, which are again comparable to the literature values (*e.g.* $Ca_{1.75}Sr_{1.5}Cu_{0.75}PtO_6$: 2.406–2.695 Å; Bykov *et al.*, 1990).

Each $Ru_{0.334}Pt_{0.666}O_6$ octahedron is connected to two Cu/O coordination polyhedra *via* a common edge (see Fig. 6), and thus chains of composition $[(Pt,Ru)_2Cu_2O_{12}]^{12-}$ are formed. The close relationship of this structure to that of the hexagonal perovskites is obvious. As depicted in Fig. 6, the Cu atoms alternately occupy sites that are shifted in the [110] and $[\overline{1}10]$ directions from the $0, 0, z$ position, and thus four cation coordination polyhedra are necessary to obtain the repeat distance in the **c** direction. The Sr ions are incorporated between the chains and provide the charge balance (see Fig. 7). These Sr ions are located at three different heights with respect to **c** (see Fig. 6). One corresponds to the z coordinate of one Cu atom, while the second and third are located at heights corresponding to the common faces of the octahedra and the copper coordination polyhedra.

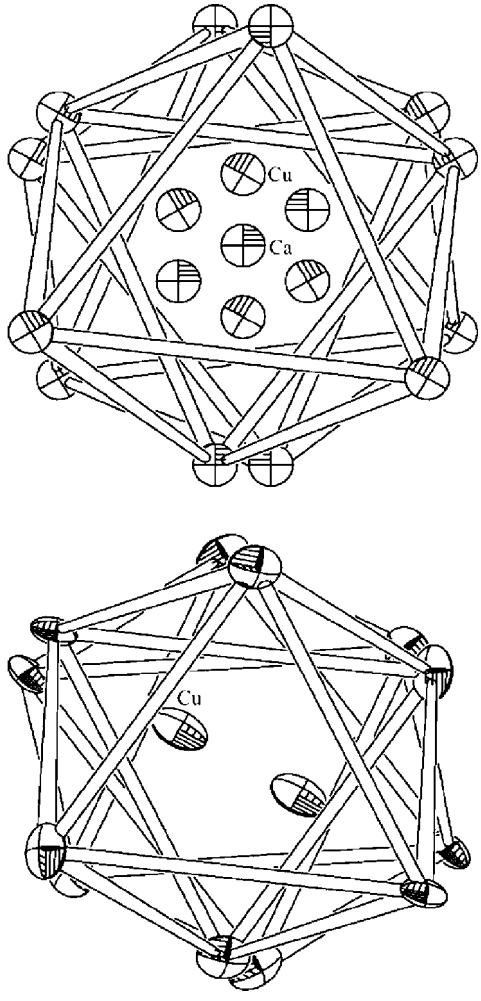

Figure 8
View of the octahedral chain in $Sr_2(Ru_{0.336},Pt_{0.664})CuO_6$ and $Ca_{1.75}Sr_{1.5}Cu_{0.75}PtO_6$. Figure drawn with *ORTEP*3 for *Windows* (Farrugia, 1997).

The bond-valence sums [calculated according to Brese & O'Keeffe (1991)] are sufficiently close to the ideal values (Table 5).

The compound most closely related to the title compound is $Ca_{1.75}Sr_{1.5}Cu_{0.75}PtO_6$ (Bykov *et al.*, 1990), which crystallizes in space group $R\overline{3}c$ with lattice parameters $a = 9.442$ and $c = 11.125$ Å. The octahedra are only occupied by Pt, yet the resulting geometry is comparable to that of the $[(Pt/Ru)O_6]$ octahedra, although in the latter the observed bond distances are slightly shorter. The Sr atoms in the title compound are supposed to be partly replaced by Ca atoms in $Ca_{1.75}Sr_{1.5}Cu_{0.75}PtO_6$, which leads to shorter cation–oxygen distances [2.41–2.58 Å for $Ca_{1.75}Sr_{1.5}Cu_{0.75}PtO_6$ *versus* 2.46–2.79 Å for $Sr_3(Ru_{0.336},Pt_{0.664})CuO_6$]. Furthermore, the coordination around the Cu atoms is also very similar.

The main difference between the two compounds is of course the lowered symmetry of $Sr_3(Ru_{0.336},Pt_{0.664})CuO_6$ with respect to $Ca_{1.75}Sr_{1.5}Cu_{0.75}PtO_6$. This difference leads to a completely ordered distribution of copper in the former compound while, according to Bykov *et al.* (1990), in the latter compound positional and occupational (Cu, Ca) disorder is observed for this site (see Fig. 8).

APPENDIX *A*

The non-standard setting $R12/c$ can be transformed to the standard setting $C2/c$ using the relationship

$$\begin{pmatrix} a' \\ b' \\ c' \end{pmatrix}_{C2/c} = \begin{pmatrix} 1/3 & -1/3 & 2/3 \\ 1 & 1 & 0 \\ -1/3 & 1/3 & 1/3 \end{pmatrix} \begin{pmatrix} a \\ b \\ c \end{pmatrix}_{R12/c}.$$

The lattice parameters for the $C2/c$ setting are $a = 9.294$, $b = 9.595$, $c = 6.679$ Å and $\beta = 92.63^\circ$. The transformed coordinates are given in the supplementary material.

The authors acknowledge the financial support of the BMBF. We are very grateful for the continuous support of Professor M. Jansen, Professor B. Keimer and Professor A. Simon.

References

Abakumov, A. M., Shpanchenko, R. V., Antipov, E. V., Lebedev, O. I., Tendeloo, G. V. & Amelinckx, S. (1998). *J. Solid State Chem.* **141**, 492–499.

Altomare, A., Cascarano, G., Giacovazzo, C., Guagliardi, A., Moliterni, A. G. G., Burla, M. C., Polidori, G., Camilli, M. & Spagna, R. (1997). *SIR*97. *A Package for Crystal Structure Solution by Direct Methods and Refinement.* University of Bari, Italy.

Boulahya, K., Parras, M. & González-Calbet, J. M. (1999). *J. Solid State Chem.* **142**, 419–427.
Brese, N. E. & O'Keeffe, M. (1991). *Acta Cryst.* B**47**, 192–197.
Bykov, A. B., Radev, S. F., Genkina, E. A., Dem'yanets, L. N., Maximox, B. A. & Melnikov, O. K. (1990). *Kristallografiya*, **35**, 869–873.
Elcoro, L., Perez-Mato, J. M. & Withers, R. (2000). *Z. Kristallogr.* **215**, 727–739.
Elcoro, L., Perez-Mato, J. M. & Withers, R. (2001). *Acta Cryst.* B**57**, 471–484.
Farrugia, L. J. (1997). *J. Appl. Cryst.* **30**, 565.
Floros, N., Michel, C., Hervieu, M. & Raveau, B. (2000). *Chem. Mater.* **12**, 3197–3201.
Gourdon, O., Petricek, V., Dusek, M., Bezdicka, P., Durovic, S., Gyepesova, D. & Evain, M. (1999). *Acta Cryst.* B**55**, 841–848.
Gourdon, O., Petricek, V. & Evain, M. (2000). *Acta Cryst.* B**56**, 409–418.
Grasset, F., Weill, F. & Darriet, J. (1998). *J. Solid State Chem.* **140**, 194–200.
Lin, C. T., Liang, B., Ulrich, C. & Bernhard, C. (2001). *Physica C*, **364/365**, 373–375.
Meyer, G., Gros, Y., Bochu, B., Collomb, A., Chenavas, J., Joubert, J. C. & Marezio, M. (1978). *Phys. Status Solidi A*, **48**, 581–>586.
Oxford Diffraction (2000). *XCALIBUR. Single Crystal Diffractometer Software*, Version 1.0. Oxford.
Palacin, M. R., Bassas, J., Rodriguez-Carvajal, J., Fuertes, A., Casan-Pastor, N. & Gomez-Romero, P. (1994). *Mater. Res. Bull.* **29**, 973–980.
Petříček, V. & Dušek, M. (2000). *JANA*2000. *Crystallographic Computing System.* Institute of Physics, Academy of the Czech Republic, Praha.
Renard, C., Daviero-Minaud, S., Huve, M. & Abraham, F. (1999). *J. Solid State Chem.* **144**, 125–135.
Stadelmann, P. A. (1987). *Ultramicroscopy*, **21**, 131.
Stoe & Cie (1998). *X-RED. Data Reduction for STADI*4 *and IPDS.* Stoe and Cie GmbH, Darmstadt, Germany.